Dual-interference-channel quantitative-phase microscopy of live cell dynamics

Natan T. Shaked,* Matthew T. Rinehart, and Adam Wax

Department of Biomedical Engineering, Fitzpatrick Institute for Photonics, Duke University, Durham, North Carolina 27708, USA

**Corresponding author: natan.shaked@duke.edu*

Received December 16, 2008; accepted January 16, 2009;
posted February 10, 2009 (Doc. ID 105428); published March 6, 2009

We introduce and experimentally demonstrate a fast and accurate method for quantitative imaging of the dynamics of live biological cells. Using a dual-channel interferometric setup, two phase-shifted interferograms of nearly transparent biological samples are acquired in a single digital camera exposure and digitally processed into the phase profile of the sample. Since two interferograms of the same sample are acquired simultaneously, most of the common phase noise is eliminated, enabling the visualization of millisecond-scale dynamic biological phenomena with subnanometer optical path length temporal stability.
© 2009 Optical Society of America
OCIS codes: 090.1995, 090.2880, 170.3880, 180.3170.

Imaging live cells requires a system that is able to visualize mostly transparent three-dimensional objects with very little inherent absorption, imposing almost no change on the light amplitude reflected from or transmitted through them. Conversely, the phase of the light transmitted through these transparent objects can give a good indication of the optical path delays associated with them. Phase imaging can be performed by several well-known microscopy techniques, such as phase contrast and differential interference contrast microscopy [1]. However, these conventional microscopy techniques do not yield quantitative phase measurements. In addition, they suffer from various artifacts that make it hard to correctly interpret the resulting phase images in terms of optical path delays.

Digital holography, on the other hand, yields quantitative measurement of the phase distribution [2–6]. Therefore, it is possible to reshape the captured complex wavefront and, for example, compensate for optical aberrations. Digital holography, however, requires interferometric setups, typically yielding phase images that are not free from phase noise. Elimination of most of the phase noise, originating from the common perturbations in the interferometer arms, the dc autocorrelation terms, and the conjugate image, can be accomplished by acquiring two or more interferograms of the same sample [5,6].

Still, certain biological processes, such as cell membrane fluctuations and neuron activity, occur faster than the scanning rates of most optical systems. Therefore, this Letter suggests an optical system for obtaining dynamic quantitative phase measurements with high precision and a low degree of phase noise. The method, called dual-interference-channel quantitative-phase microscopy (DQPM), is based on a dual-channel interferometric setup that is able to simultaneously obtain two phase-shifted interferograms of the same sample. These interferograms are digitally processed to yield the phase profile of the sample. Owing to the fact that two interferograms of the same sample are acquired, it is possible to eliminate most of the common phase noise in the final phase image. Additionally, owing to the simultaneous manner of the acquisition, one can capture rapid cell phenomena with subnanometer temporal stability, with the only limit being the true full frame rate of the digital camera used.

Ikeda *et al.* [7] have suggested another dynamic quantitative phase microscopy method that is based on the acquisition of a single interferogram. While this method avoids temporal phase noise between successive frames, spatial filtering must then be used to eliminate the dc autocorrelation terms (which can also cause phase errors). In addition, since the interferogram is acquired in a highly off-axis geometry in order to separate the dc autocorrelation terms from the signal, there is potential for losing high-frequency components in the sample field. Various attempts for simultaneous phase imaging have been performed in the optical testing field [8–12]. However, these methods are not implemented for microscopy of biological cells as performed in the current Letter.

Figure 1 illustrates the DQPM system. This system includes an off-axis digital holographic microscopy setup based on a Mach–Zehnder interferometer, followed by an image splitting system. Light from a He–Ne laser source, linearly polarized at 45°, is split into sample and reference beams by beam splitter BS_1. The sample arm includes a biological sample and microscope objective MO that is in a 4*f* configuration with lens L_2. Lens L_1 in the reference arm is in a 4*f* configuration with lens L_2 as well. BS_2 combines the sample and reference beams, and the interference pattern of interest appears one focal length behind lens L_2. This interference pattern is spatially restricted by an aperture to an area that is not bigger than half of the digital camera sensor size. The interference pattern at the aperture plane is then imaged, through the 4*f* image splitting system shown in Fig. 1(b), onto the digital camera. This 4*f* image splitting system includes two identical lenses, L_3 and L_4, creating a one-to-one image of the aperture plane onto

 © 2009 Optical Society of America

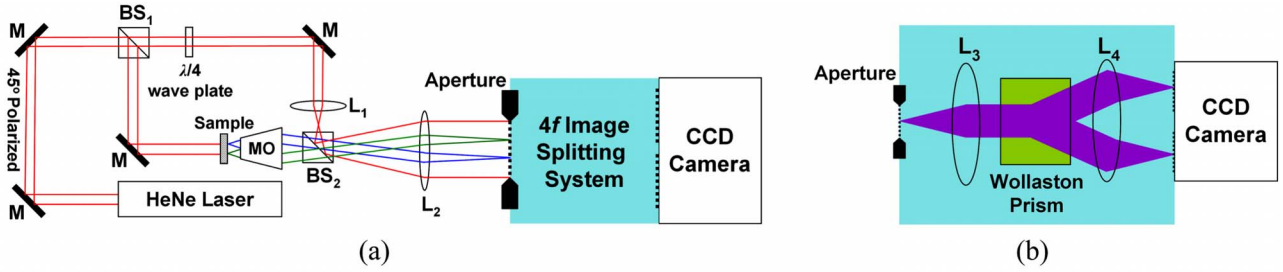

Fig. 1. (Color online) DQPM system. Dual-channel single-exposure interferometer for obtaining phase profiles of live dynamic biological cells: (a) entire interferometer, (b) 4*f* image splitting system.

the camera. A Wollaston prism is positioned between these two lenses to create two spatially separated and phase-shifted interferograms on the camera.

The phase shift between the interferograms is explained as follows. In the reference arm, a quarter ($\lambda/4$)-wave plate is oriented along the horizontal axis, so that the light transmitted through it has 90° phase difference between the horizontal and vertical components. On the other hand, in the sample arm the light remains 45° linearly polarized, so there is 0° phase difference between the horizontal and vertical components. When the beams are combined by BS_2, there is $\alpha = 90°$ shift between the interference pattern formed by the horizontal component and the interference pattern formed by the vertical component. Owing to its ability to output two perpendicularly polarized beams, the Wollaston prism separates the horizontal or vertical components for each of the interferograms, yielding a phase shift of α between the interferograms.

The two interferograms, I_1 and I_2, acquired by the digital camera in a single exposure, can be mathematically expressed as follows:

$$I_1 = I_R + I_S + 2\sqrt{I_S I_R}[\cos(\varphi_{\mathrm{OBJ}} + \varphi_{\mathrm{C}})],$$

$$I_2 = I_R + I_S + 2\sqrt{I_S I_R}[\cos(\varphi_{\mathrm{OBJ}} + \varphi_{\mathrm{C}} + \alpha)], \quad (1)$$

where I_R and I_S are the reference and sample intensity distributions, respectively; φ_{OBJ} is the spatially varying phase associated with the object; and φ_{C} is the spatially varying phase of the interferometer without the presence of the object. Note that φ_{C} and α can be digitally measured, based on the fact that slightly off-axis holographic geometry is used, by fitting the background interference (interference pattern observed without the presence of the sample) in each of the interferograms to a sine wave. The wrapped object phase φ_{OBJ} is computed as follows:

$$F = \frac{\exp(-j\varphi_{\mathrm{C}})}{1 - \exp(j\alpha)}[I_1 - I_2 + j\mathrm{HT}\{I_1 - I_2\}],$$

$$\varphi_{\mathrm{OBJ}} = \arctan\left\{\frac{\mathrm{Im}\, F}{\mathrm{Re}\, F}\right\}, \quad (2)$$

where HT denotes a Hilbert transform. Next, an unwrapping algorithm is applied to obtain the final unwrapped object phase. Note that the process described above removes most common noise and background elements, enabling reliable phase measurement. In addition, since the interferograms I_1 and I_2 are acquired simultaneously, in a nonscanning manner, fast phenomena can be visualized.

To demonstrate the DQPM system shown in Fig. 1, we have imaged a live, unstained MDA-MB-468 human breast cancer cell in standard phenol red growth medium. Figure 2(a) shows the regular microscopic image of the sample through the optical system, demonstrating the very low visibility achieved with simple imaging of this sample. A He–Ne laser (5 mW, 633 nm) was used as the source in the interferomet-

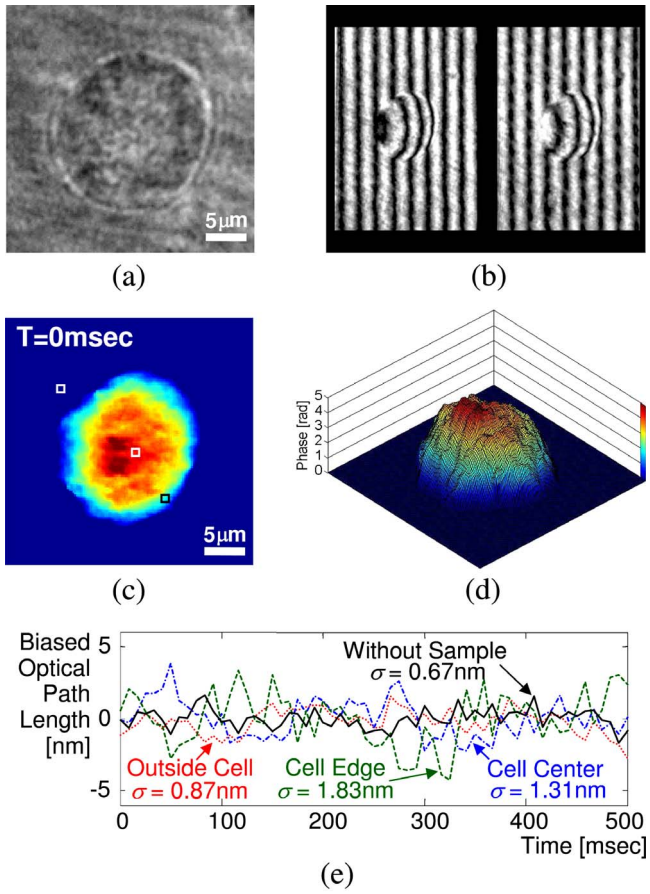

Fig. 2. (Color online) MDA-MB-468 human breast cancer cell. (a) Regular microscopic imaging through the system. (b) Two phase-shifted interferograms captured in a single camera exposure. (c) Final unwrapped phase profile (Media 1). (d) Surface plot of the phase profile shown in (c). (e) Temporal phase stability without the sample and with the sample in the three points marked in (c). Viewing this figure in color online is highly recommended.

ric setup. In both interferometer arms, 40×, 0.65 NA achromatic objective lenses were used. Each of these lenses created 33× magnification when paired with lens L_2 (15 cm focal length). The resulting complex amplitude was spatially restricted by a 3.2 mm ×2.3 mm aperture. The 4*f* image splitting system shown in Fig. 1(b) used two similar lenses L_3 and L_4, each with a focal length of 7.5 cm. The Wollaston prism (crystal quartz, 2° of angular separation), positioned between these two lenses, split the pattern from the aperture plane so that the CCD camera (AVO Pike F032-B, 640×480 pixels) captured the two phase-shifted interferograms I_1 and I_2 shown in Fig 2(b), spatially separated by about 2.4 mm. To determine the coordinate mapping between the two different interferograms in the single CCD image, a test target (U.S. Air Force resolution chart) was used as a preprocessing sample. The frequency q and the actual phase shift α were extracted by fitting each of the interferograms to a sine wave. Based on the fact that the background interference fringes in each of the interferograms are vertical, we get $\varphi_C = qx$, where x is the horizontal coordinate in each interferogram frame. Figures 2(c) and 2(d) show the final unwrapped phase profile of the sample as obtained by applying Eq. (2) and a phase-unwrapping algorithm. The same cell was acquired every 8.3 ms [120 frames per second (fps)] for a duration of 500 ms. As can be seen from Media 1 [Fig. 2(c)], the temporal phase stability is excellent even in the presence of a sample containing fluid media.

To quantify this temporal phase stability, we recorded the temporal path-length fluctuations, associated with a diffraction-limited spot defined by the imaging optics, on the millisecond time scale. The stability was first assessed without the presence of a sample, and then with the presence of the sample in the three marked points in Fig. 2(c): on the cell center, on the cell edge, and at the background (through the medium only). The fluctuations standard deviations in these four cases were 0.67 nm, 1.31 nm, 1.83 nm, and 0.87 nm, respectively, as shown in Fig. 2(e). The first result above, representing the true temporal stability of the optical system, indicates that subnanometer path-length sensitivity can be achieved for imaging on the millisecond time scale. We attribute the slightly lower stability in the three latter cases to small vibrations occurring inside the entire sample.

To illustrate the utility of DQPM for imaging dynamic cell phonemena, Media 2 (Fig. 3) (120 fps acquired for 2 s) presents the phase profiles of a rat beating myocyte (myocardial cell taken from rat heart muscles) in phenol red growth medium.

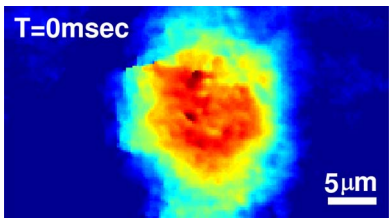

Fig. 3. (Color online) Final unwrapped phase profile of a rat beating myocyte (Media 2). Viewing this figure in color online is highly recommended.

In summary, we have demonstrated a method for imaging fast biological phenomena with high accuracy. Experimental results show good spatial resolution for dynamic cell phase imaging and excellent temporal phase stability. Owing to its simultaneous acquisition, the system's ability to observe fast cellular phenomena is limited only by the true full frame rate of the camera, and thus this method provides a powerful tool for dynamic studies of biological cells.

We thank Nenad Bursac and Lisa Satterwhite for providing us with myocyte samples. This work was supported by grants from the National Institutes of Health (NIH) (NCI R33-CA109907), the National Science Foundation (NSF) (BES 03-48204). N.T.S. greatly acknowledges the support of the Bikura Postdoctoral Fellowship from Israel.

References

1. M. Pluta, *Advanced Light Microscopy* (Elsevier Science Publishing, 1988), Vol. 2.
2. T. Zhang and I. Yamaguchi, Opt. Lett. **23**, 1221 (1998).
3. E. Cuche, F. Bevilacqua, and C. Depeursinge, Opt. Lett. **24**, 291 (1999).
4. P. Marquet, B. Rappaz, P. J. Magistretti, E. Cuche, Y. Emery, T. Colomb, and C. Depeursinge, Opt. Lett. **30**, 468 (2005).
5. G. Popescu, L. P. Deflores, J. C. Vaughan, K. Badizadegan, H. Iwai, R. R. Dasari, and M. S. Feld, Opt. Lett. **29**, 2503 (2004).
6. K. J. Chalut, W. J. Brown, and A. Wax, Opt. Express **15**, 3047 (2007).
7. T. Ikeda, G. Popescu, R. R. Dasari, and M. S. Feld, Opt. Lett. **30**, 1165 (2005).
8. J. Muñoz, M. Strojnik, and G. Páez, Appl. Opt. **42**, 6846 (2003).
9. N. Brock, J. Hayes, B. Kimbrough, J. Millerd, M. North-Morris, M. Novak, and J. Wyant, Proc. SPIE **5875**, 58750F (2005).
10. Y. Zhu, L. Liu, Y. Zhi, Z. Luan, and D. Liu, Proc. SPIE **6671**, 66711D (2007).
11. T. Kiire, S. Nakadate, and M. Shibuya, Appl. Opt. **47**, 4787 (2008).
12. G. Rodriguez-Zurita, N. Toto-Arellano, C. Meneses-Fabian, and J. F. Vázquez-Castillo, Opt. Lett. **33**, 2788 (2008).